Dynamical scaling analysis of symmetry breaking for the antiferromagnetic triangular Heisenberg model in a uniform magnetic field

Kazuaki Murayama[1] and Yukiyasu Ozeki[2]

[1]*Department of Computer and Network Engineering, Graduate School of Informatics and Engineering, The University of Electro-Communications, 1-5-1 Chofugaoka, Chofu-shi, Tokyo 182-8585, Japan*

[2]*Department of Engineering Science, Graduate School of Informatics and Engineering, The University of Electro-Communications, 1-5-1 Chofugaoka, Chofu-shi, Tokyo 182-8585, Japan*

(Received 10 February 2020; revised manuscript received 6 May 2020; accepted 11 May 2020; published 26 May 2020)

Phase transitions for the two-dimensional antiferromagnetic triangular Heisenberg model in a uniform field are primarily analyzed using dynamical scaling analysis. The system has Z_3 and $O(2)$ symmetries. The transition temperatures and types of transition are investigated using the relaxation of order parameters and the asymptotic behaviors of relaxation time around transition temperatures. In the low-field range, the order parameters for the Z_3 and $O(2)$ symmetries exhibit the behavior typical of a second-order transition and Kosterlitz-Thouless (KT) transition, respectively, with distinct transition temperatures. In the high-field range, an order parameter for the Z_3 symmetry exhibits the behavior of a second-order transition, while another order parameter related to the components perpendicular to the field demonstrates that the relaxation time diverges with an asymptotic form, indicating a second-order transition rather than a KT transition. These transition temperatures are estimated to be close. Critical exponents for these two order parameters are estimated separately by calculating the relaxation of fluctuations in the high-field range. It was confirmed that the critical exponents for both of these order parameters change continuously as a function of field, and they are distinct from each other.

DOI: 10.1103/PhysRevB.101.184427

I. INTRODUCTION

Elucidation of frustrated systems is a major issue in condensed matter and statistical physics because complicated ordered phases appear under the influence of frustration [1,2]. The antiferromagnetic (AF) triangular Heisenberg model has been extensively studied for both quantum and classical systems [3–11]. $RbFe(MoO_4)_2$ [12] and $Rb_4Mn(MoO_4)_3$ [13] have been established as the materials corresponding to this system.

At the zero field, this system assumes a 120 degree structure in the ground state [3]. There is a Z_2 vortex, which causes a phase transition of the binding-unbinding property of vortices [3,14,15]. In the nonzero fields, the model has previously been investigated using the equilibrium Monte Carlo simulation (EMCS), and the phase diagram was obtained in the temperature-field plane [4,5,16]. The phase diagram is briefly shown in Fig. 1. Double ordered phases were reported in the low-field range ($0 \lesssim h \lesssim 3$) [16]. The Y phase is associated with Z_3 breaking and algebraic ordering of $O(2)$ [4,5,16]. The up-up-down (UUD) phase involves only Z_3 breaking, and this phase was called the one-third magnetization plateau in Ref. [16]. The Kosterlitz-Thouless (KT) transition [17,18] in terms of $O(2)$ occurs between the Y phase and UUD phase. A second-order transition breaking Z_3 occurs between the UUD phase and the paramagnetic (PM) phase, and this transition belongs to the same universality class as the three-state Potts model. In the high-field range ($3 \lesssim h \lesssim 9$), a single ordered phase called the 2:1 canted phase was reported [16]. A single phase transition in terms of Z_3 and $O(2)$ occurs between this phase and the PM phase. At the transition temperature, there was a nonuniversal jump in the spin stiffness, which detects the transition in terms of $O(2)$, and the critical exponents for both the Z_3 and $O(2)$ symmetries change continuously as a function of the field and do not belong to any universality class [16].

An important problem of the system is that the transitions in the high and low fields are distinct. Although previous studies [4,5,16] confirm a picture of the phase transitions in the low-field range, few studies have reported on the nature of the transitions in the high-field range. In this study, we primarily analyze the phase transition between the 2:1 canted phase and PM phase in the high-field range. The phase transition between the UUD phase and 2:1 canted phase is beyond the scope of this study. To compare the phase transition in the high-field range with that in the low-field range, we also analyze the transition temperature and transition type between the UUD phase and PM phase and those between the Y phase and UUD phase in the low-field range.

We study the system using the nonequilibrium relaxation (NER) method: a numerical method for analyzing equilibrium phase transitions [19]. In this method, equilibrium properties can be analyzed using a dynamical behavior from a fully ordered initial state to the equilibrium one. Such a data of dynamical behavior is identical to one discarded as the equilibration in the EMCS. Because the NER method has been successful with frustrated and random systems [20–22], we expect that this method will be effective for the present

system. An advantage of analysis using the NER method over EMCS is that the behavior of the thermodynamic limit can be realized even at around the transition temperature where the fluctuation becomes large. This is because the calculation is terminated before the correlation length $\xi(t)$ reaches the edge of the size at which the finite-size effect occurs. Notwithstanding slowly relaxing systems due to the frustration, the NER method does not require calculations to derive the equilibrium state. Consequently, computational resources are allocated to enlarging the system size.

The structure of the paper is as follows: In Sec. II, details of the model and the dynamical order parameters are defined. In Sec. III, dynamical scaling for NER data is applied to the phase transitions in the low-field range, and we obtain results for transition temperatures, dynamical exponents, and transition types. Comparing these results with those from previous studies [4,5,16], we provide a basis for analysis in the high-field range. In Sec. IV, results for transitions in the high-field range are presented. Transition temperatures, dynamical exponents, and transition types are obtained. Furthermore, static critical exponents are estimated for order parameters by investigating the relaxation of fluctuations. In Sec. V, we discuss our results.

II. MODEL

We consider the classical AF Heisenberg model:

$$\mathcal{H} = -J \sum_{\langle ij \rangle} \boldsymbol{S}_i \cdot \boldsymbol{S}_j - h \sum_i S_i^z, \tag{2.1}$$

where the summation $\langle ij \rangle$ runs over all nearest-neighbor sites on the triangular lattice. A uniform magnetic field h is applied along S^z components, and J assumes a negative value due to AF interaction and is set as $J = -1$. We measure the temperature T and uniform field h in units of J/k_B and J, respectively.

First, we consider the ground state and the spin structure in the zero-temperature limit. To explain the ground state, the spin structure, and order parameters, it is convenient to use the concepts of a sublattice and plaquette. As seen in Fig. 2, the triangular lattice is divided into three sublattices A, B, and C. The three spins on a plaquette satisfy

$$\boldsymbol{S}_A + \boldsymbol{S}_B + \boldsymbol{S}_C = \left(0, 0, \frac{h}{3}\right), \tag{2.2}$$

for $0 \leqslant h \leqslant 9$ in the ground state [4]. At the zero field, the system assumes a 120 degree structure, which certainly satisfies Eq. (2.2). In the nonzero fields, the system does not assume the pure 120 degree structure in the zero-temperature limit. Based on spin-wave analysis [23,24], the spin structure in the zero-temperature limit is obtained as

$$\theta_A = \cos^{-1}\{(h+3)/6\}, \tag{2.3}$$

$$\theta_B = -\theta_A, \tag{2.4}$$

$$\theta_C = -\pi, \tag{2.5}$$

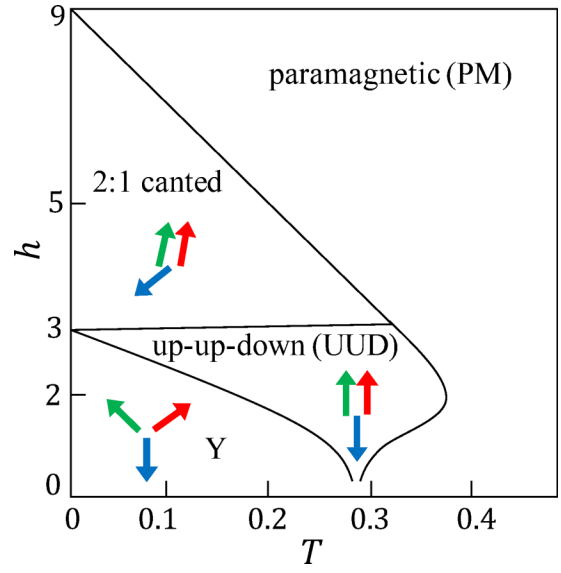

FIG. 1. Conceptual illustration of phase diagram of the AF triangular Heisenberg model expected by previous studies [4,5,16].

for $0 < h \leqslant 3$, and

$$\theta_A = \cos^{-1}\left\{\left(h^2 + 27\right)/12h\right\}, \tag{2.6}$$

$$\theta_B = \theta_A, \tag{2.7}$$

$$\theta_C = -\cos^{-1}\left\{\left(h^2 - 27\right)/6h\right\}, \tag{2.8}$$

for $3 \leqslant h \leqslant 9$, where θ_X, with $X = A$, B, or C, is a polar angle of the spin variable $\boldsymbol{S}_X$ measured from the z axis along the S^z direction. For example, the structures for $h = 2$, 3, and 5, which are used later as initial states of order parameters, are shown in Fig. 3. To obtain these structures, first S^z is determined from Eqs. (2.3)–(2.8), then setting $S^x = 0$, S^y is calculated using $|\boldsymbol{S}| = 1$.

Next, we consider the spin structures in ordered phases. In the low-field range, a collinear UUD structure is realized in the UUD phase in which the $O(2)$ symmetry remains while Z_3 is broken [4,5,16]. In the Y phase, the spins form a coplanar structure with a canted 120 degree structure [4,5,16]. In the high-field range, the spins also form a coplanar structure in the 2:1 canted phase. However, they have a different structure.

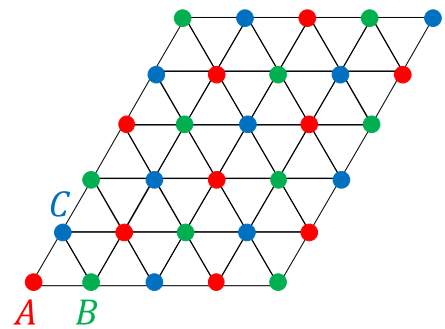

FIG. 2. Conceptual illustration of the two-dimensional triangular lattice at a size of 6×5. The red, green, and blue sites denote three sublattices A, B, and C, respectively.

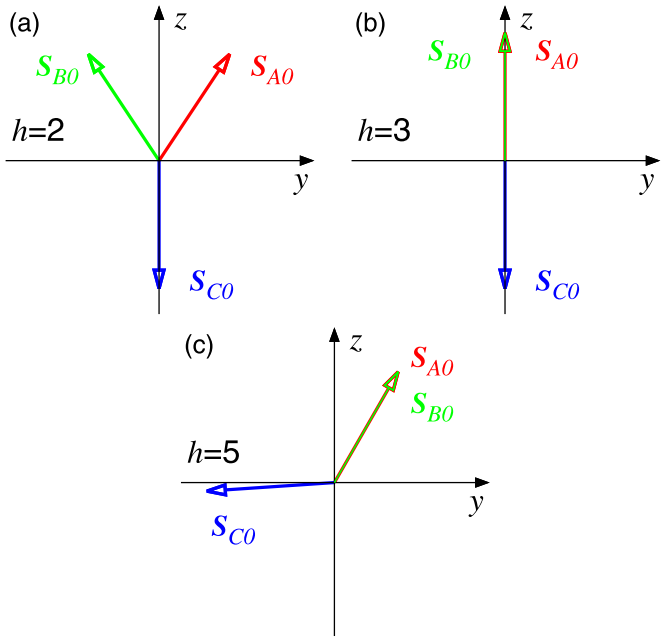

FIG. 3. The spin structures in the zero-temperature limit in the case of $S^x = 0$. (a) That for $h = 2$; $\boldsymbol{S}_{A0} = (0, \sqrt{1-(5/6)^2}, 5/6)$, $\boldsymbol{S}_{B0} = (0, -\sqrt{1-(5/6)^2}, 5/6)$, and $\boldsymbol{S}_{C0} = (0, 0, -1)$. (b) That for $h = 3$; $\boldsymbol{S}_{A0} = \boldsymbol{S}_{B0} = (0, 0, 1)$ and $\boldsymbol{S}_{C0} = (0, 0, -1)$. (c) That for $h = 5$; $\boldsymbol{S}_{A0} = \boldsymbol{S}_{B0} = (0, \sqrt{1-(13/15)^2}, 13/15)$ and $\boldsymbol{S}_{C0} = (0, -\sqrt{1-(1/15)^2}, -1/15)$.

Two spins on a plaquette are parallel to each other and canted to the remaining spin.

Here, we explain the order parameters. To analyze a phase transition using NER analysis, we introduce dynamical order parameters that assume a finite value in a low-temperature phase and disappear in a high-temperature phase. They are defined for a fully ordered state that maximizes their values and are calculated from that state. We denote such a state as $\boldsymbol{S}_{X0} = (S^x_{X0}, S^y_{X0}, S^z_{X0})$. An order parameter for the S^z components in terms of the Z_3 symmetry is

$$\psi = \frac{3}{8N}\left\{\sum_A 2S^z_A + \sum_B 2S^z_B - \sum_C 4S^z_C\right\}, \tag{2.9}$$

where the summations for A, B, and C run over all $N/3$ elements on the sublattices. Equation (2.9) is part of the complex order parameter used in a previous study [16]. The other order parameter for the S^x-S^y components in terms of the $O(2)$ symmetry is defined as

$$m_{xy} = \frac{2}{N}\left\{\sum_A \boldsymbol{S}^\perp_A \cdot \boldsymbol{S}^\perp_{A0} + \sum_B \boldsymbol{S}^\perp_B \cdot \boldsymbol{S}^\perp_{B0} + \sum_C \boldsymbol{S}^\perp_C \cdot \boldsymbol{S}^\perp_{C0}\right\}, \tag{2.10}$$

where $\boldsymbol{S}^\perp_X = (S^x_X, S^y_X)$ is a two-dimensional vector defined by removing the S^z component from the spin variable. Removing the S^z component, the behavior of the S^x-S^y components around the field axis can be observed. By substituting

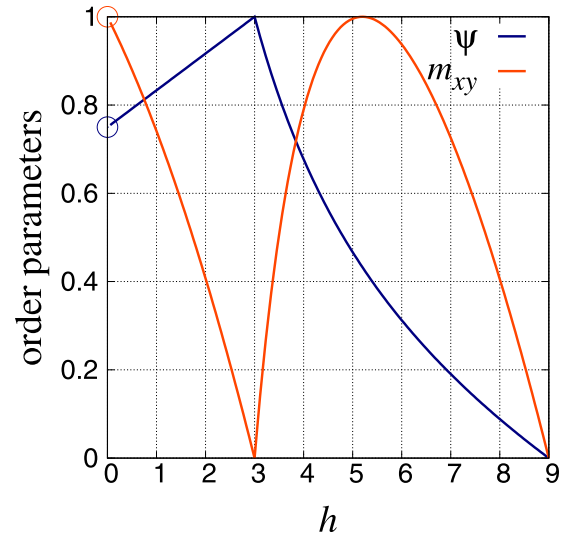

FIG. 4. Two order parameters are plotted as a function of h in the zero-temperature limit.

Eqs. (2.3)–(2.8) into Eqs. (2.9) and (2.10) setting $\boldsymbol{S}^\perp_{X0} = \boldsymbol{S}^\perp_X$, these order parameters can be expressed as a function of field:

$$\psi = \frac{h+9}{12}, \tag{2.11}$$

$$m_{xy} = \frac{4}{3}\left\{1 - \left(\frac{h+3}{6}\right)^2\right\}, \tag{2.12}$$

for $0 < h \leqslant 3$, and

$$\psi = \frac{3}{8}\left(\frac{9}{h} - \frac{h}{9}\right), \tag{2.13}$$

$$m_{xy} = 4\left\{1 - \left(\frac{h^2+27}{12h}\right)^2\right\}, \tag{2.14}$$

for $3 \leqslant h \leqslant 9$. These order parameters in the zero-temperature limit are plotted in Fig. 4.

III. LOW-FIELD RANGE

First, we analyze the phase transition in the low-field range, typically at $h = 2$, and confirm that dynamical scaling analysis using the dynamical order parameters defined above produces results consistent with the results of previous studies [4,5,16]. ψ is used to analyze that between the UUD phase and PM phase. m_{xy} is intended for that between the Y phase and UUD phase.

A. Relaxation of order parameters

To investigate asymptotic behaviors for relaxation of the order parameters and to perform dynamical scaling analysis, we calculate relaxation of ψ and m_{xy} at $h = 2$. Figure 3(b) is selected as the initial state for ψ. Although it is the structure in zero-temperature limit at $h = 3$, this structure is realized in the UUD phase as shown in Fig. 1 and it is reasonable to select it as the initial state for ψ at $h = 2$. That for m_{xy} is selected as Fig. 3(a). The heat bath algorithm [25] is used for this system up to 10^4 Monte Carlo steps (MCSs). We note that a Monte

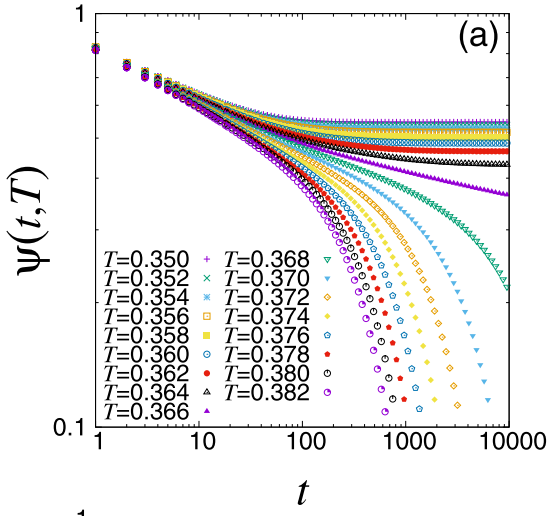

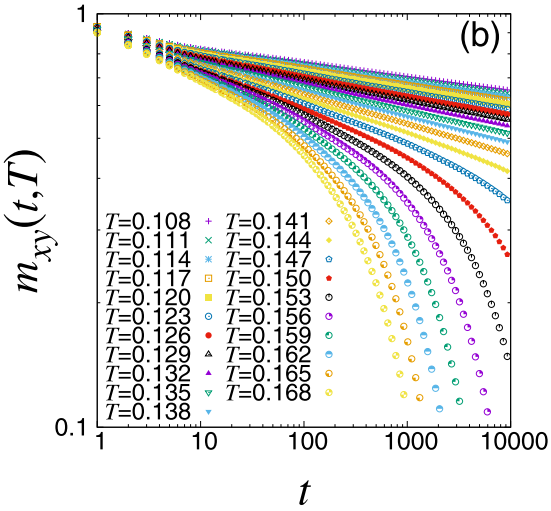

FIG. 5. Relaxation of the order parameters at $h = 2$ on the 2001×2000 triangular lattice plotted on a double-logarithmic scale. (a) The relaxation of ψ. (b) That of m_{xy}.

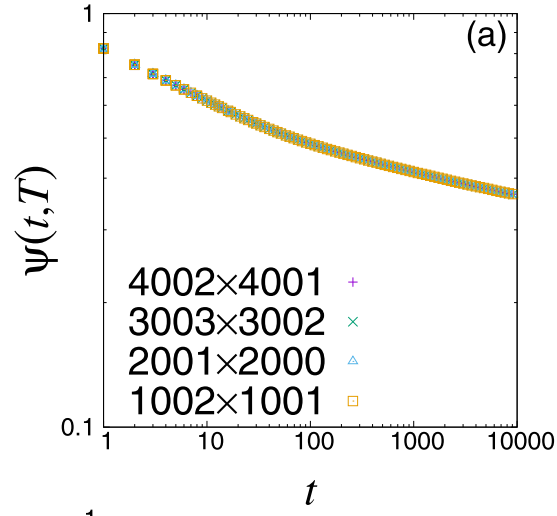

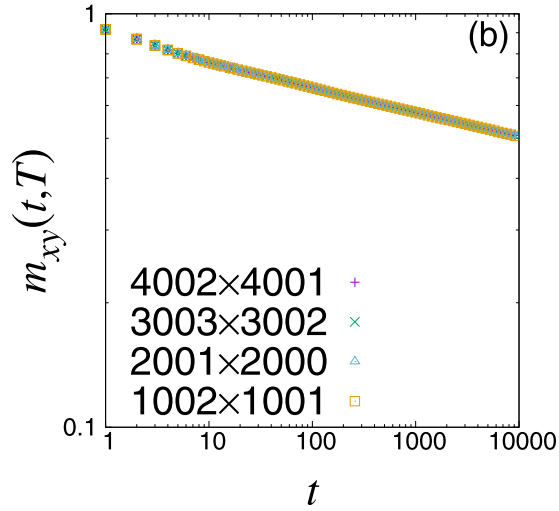

FIG. 6. The size dependence of relaxation close to the transition temperature. (a) The relaxation of ψ at $(T, h) = (0.366, 2)$. (b) That of m_{xy} at $(T, h) = (0.136, 2)$. For the case $L = 1001$, the relaxation coincides with those for larger sizes, 2000, 3002, 4001, up to 10^4 MCSs.

Carlo step is defined by a single update per spin. The system size is 2001×2000 on the triangular lattice, and the skew boundary condition [26] is used. For statistical averaging, 864 independent samples are taken at several temperatures around the transition point. The results are plotted in Fig. 5 with a double-logarithmic scale. Hereafter, dynamical order parameters are plotted as normalized by the value of the initial state; this does not affect the appearance of the data because the initial state is identical in each plot. To check the size dependence, relaxation is also calculated for several sizes at $T = 0.366$ for ψ and at $T = 0.136$ for m_{xy}, close to the transition temperatures [16] where fluctuations become large. The results are shown in Fig. 6. We confirm that the finite-size effect does not appear up to 10^4 MCSs on the 2001×2000 triangular lattice.

According to the standard NER analysis [19], it is expected that the asymptotic behavior of the order parameter (say m in general) is expected to be

$$m(t, T) \sim \begin{cases} m_{\rm eq} & (T < T_{\rm c}), \\ t^{-\lambda_m} & (T = T_{\rm c}), \\ \exp\left[-t/\tau(T)\right] & (T > T_{\rm c}), \end{cases} \tag{3.1}$$

for a second-order transition, and

$$m(t, T) \sim \begin{cases} t^{-\lambda_m(T)} & (T \leqslant T_{\rm KT}), \\ \exp\left[-t/\tau(T)\right] & (T > T_{\rm KT}), \end{cases} \tag{3.2}$$

for a KT transition, where λ_m is a dynamical exponent and $\tau(T)$ is a relaxation time depending on the temperature. In Fig. 5(a), ψ exhibits the same behavior as a relaxation of a second-order transition like Eq. (3.1). In Fig. 5(b), m_{xy} decays exponentially in the high-temperature range, indicating a downward trend, while it is not clear whether m_{xy} is relaxing toward a spontaneous order like Eq. (3.1) or with a power-law decaying like Eq. (3.2) in the low-temperature range. A transition type of m_{xy} cannot be distinguished clearly only from the observation in Fig. 5(b).

B. Dynamical scaling analysis and determination of transition type

The dynamical scaling analysis is necessary to estimate the transition temperature and a dynamical exponent. In this

subsection, this analysis is used to examine the transition type of m_{xy} shown in Fig. 5(b). The dynamical scaling law is expressed as

$$m(t,T) = \tau(T)^{-\lambda_m}\Psi\left(\frac{t}{\tau(T)}\right), \tag{3.3}$$

where λ_m is a dynamical exponent and $\tau(T)$ represents a relaxation time; these are given as

$$\lambda_m = \beta/z\nu, \tag{3.4}$$

$$\tau(T) = a|T - T_c|^{-b}, \tag{3.5}$$

for a second-order transition where β, z, and ν are critical exponents associated with the order parameter, relaxation time, and correlation length, respectively. These exponents and $b = z\nu$ are universal quantities, and a in Eq. (3.5) is a nonuniversal amplitude [19]. For a KT transition,

$$\lambda_m = \eta/2z, \tag{3.6}$$

$$\tau(T) = a\exp\left(\frac{b}{\sqrt{T - T_{KT}}}\right) \tag{3.7}$$

are used instead of Eqs. (3.4) and (3.5), where η is associated with the correlation function, which is a universal quantity, and a in Eq. (3.7) is a nonuniversal amplitude. It is not clear whether b in Eq. (3.7) is a universal quantity or not [19]. We note that Eqs. (3.6) and (3.7) are only valid over a temperature range outside the KT phase. The relaxation data are converted according to the following formula:

$$X_i = t_i/\tau_i, \tag{3.8}$$

$$Y_i = \tau_i^{\lambda_m} m(t_i, T_i), \tag{3.9}$$

$$E_i = \tau_i^{\lambda_m} \delta m(t_i, T_i), \tag{3.10}$$

where E_i expresses the statistical error of Y_i. These data should collapse on a dynamical scaling function as

$$Y_i = \Psi(X_i). \tag{3.11}$$

To perform the scaling analysis according to Eq. (3.3), it is necessary to select an asymptotic form of the relaxation time $\tau(T)$ as Eq. (3.5) or Eq. (3.7). As seen in Fig. 5(a), the relaxation of ψ indicates a behavior typical of a second-order transition, i.e., Eq. (3.1); then, we will use Eq. (3.5) for this order parameter. On the other hand, it is not clear whether m_{xy} in Fig. 5(b) follows the behavior of the second-order transition or that of the KT transition. To identify the behavior, the analysis for discriminating the transition type [27,28] is applied, where comparisons of relaxation times are performed on data of m_{xy}. Three types of dynamical scaling are required for this analysis. The first type is a dynamical scaling with the relaxation time of the second-order transition, Eq. (3.5). The second type uses that of the KT transition, Eq. (3.7), and in the third, a function for the relaxation time is not assumed regarding $\tau(T)$ in Eq. (3.3) as a parameter depending on temperature. We applied this analysis to data of m_{xy} for eleven values of temperature in the high-temperature range, i.e., $T_1 = 0.138, T_2 = 0.141, \ldots, T_{11} = 0.168$. We use data only in the high-temperature range because the KT transition is assumed

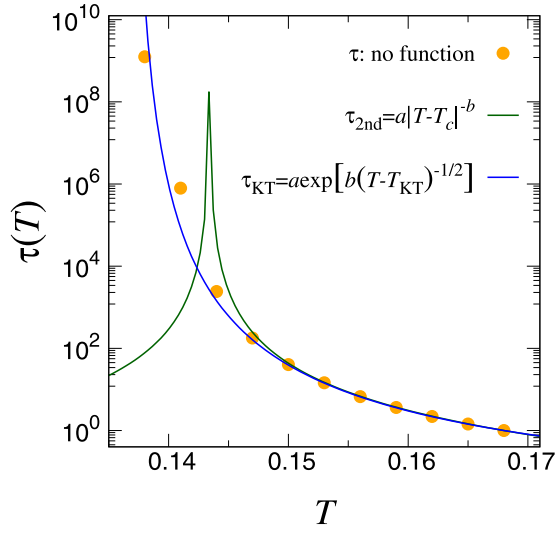

FIG. 7. Comparison of relaxation times estimated by three types of dynamical scaling for m_{xy} in Fig. 5(b) at $h = 2$. They are plotted versus T.

in one of the scalings. We choose several data points after 100 MCSs at regular intervals on $\ln(t)$ for each temperature. The method of dynamical scaling automated by Bayesian estimation and the kernel method is used [27]. In the first and second scaling with an assumed function, the relaxation time is obtained by substituting the estimated parameters (a, b, T_c, and T_{KT}) in Eqs. (3.5) and (3.7). In addition, τ_ℓ for T_ℓ ($\ell = 1, \ldots, 11$) are also estimated in the third scaling without assuming a function. The result is shown in Fig. 7. It is expected that values of τ_ℓ estimated without assuming a function are the most reliable. As seen in Fig. 7, these values seem to be in good agreement with the curve obtained by using Eq. (3.7) for the KT transition. Furthermore, the numerical difference between $\tau(T_\ell)$ with assuming functions and τ_ℓ is also evaluated. The study in Ref. [27] proposes evaluating a numerical difference using a residual defined by

$$r = \frac{1}{N_T}\sum_{\ell=1}^{N_T}\{\ln\tau(T_\ell) - \ln\tau_\ell\}^2, \tag{3.12}$$

where $\tau(\cdot)$ obeys Eq. (3.5) or Eq. (3.7), and $N_T = 11$ is the number of temperatures. The residuals are calculated as $r_{KT} = 1.43$ for Eq. (3.7) and $r_{2nd} = 3.01 \times 10^1$ for Eq. (3.5) indicating that m_{xy} in Fig. 5(b) exhibits the behavior of a KT transition in the high-temperature range. Therefore, that in the low-temperature range should exhibit the behavior of a KT phase, which decays in a power law, not toward a spontaneous order.

C. Estimation of transition temperature and dynamical exponent

In this subsection, the transition temperature and the dynamical exponent are estimated using the dynamical scaling analysis introduced in Sec. III B. Several temperatures in which the relaxation clearly show a downward trend regarded as in a high-temperature phase are selected for ψ shown in Fig. 5(a) and m_{xy} shown in Fig. 5(b). Similarly, several

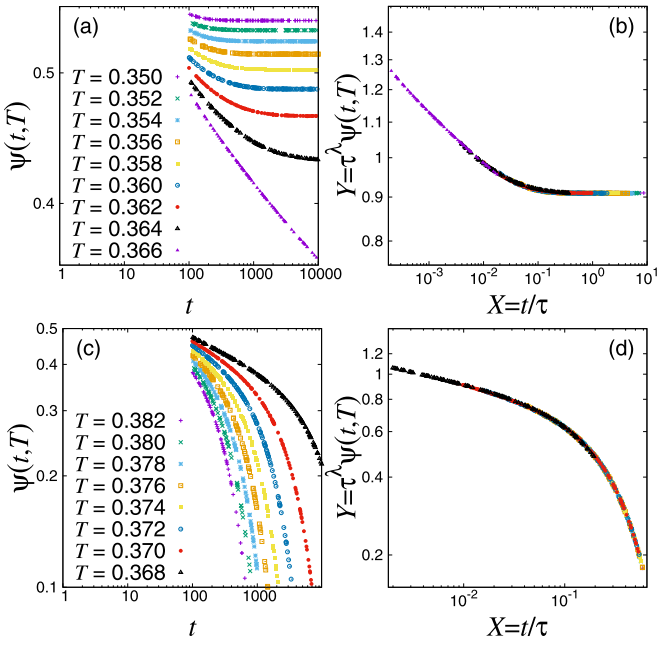

FIG. 8. (a) An example of randomly chosen relaxation data of ψ in the low-temperature range in Fig. 5(a), and (b) corresponding scaling plot. (c), (d) Those in the high-temperature range.

temperatures in which relaxation clearly show an upward trend regarded as in a low-temperature phase are also selected for ψ shown in Fig. 5(a). In Sec. III B for the comparison of the relaxation time, temperatures close to the transition point were actively used to identify the asymptotic form of the relaxation time. However, those temperatures are avoided here because such data very close to the transition point sometimes make the fitting procedure difficult and affect the accuracy of estimations. Several data points are randomly chosen for each temperature after 100 MCSs. Assuming Eq. (3.5) for ψ, dynamical scaling analysis is performed to estimate its T_c and λ_m. Those of m_{xy} are also estimated with the same analysis, assuming Eq. (3.7) for it. We note that the same algorithm applied in Sec. III B is also used, and the analysis is performed separately for the low and the high temperature ranges for ψ, and only for the high-temperature range for m_{xy}. The results are shown in Fig. 8 for ψ and Fig. 9 for m_{xy}.

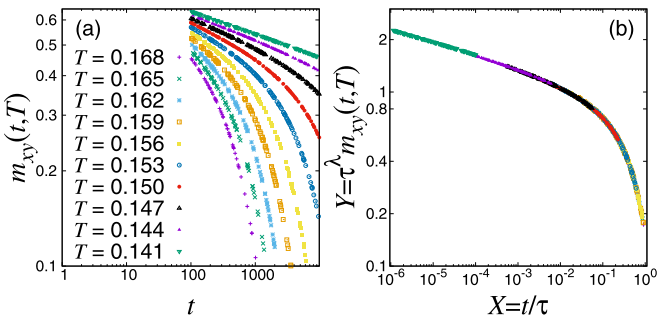

FIG. 9. (a) An example of randomly chosen relaxation data of m_{xy} in the high-temperature range in Fig. 5(b), and (b) corresponding scaling plot.

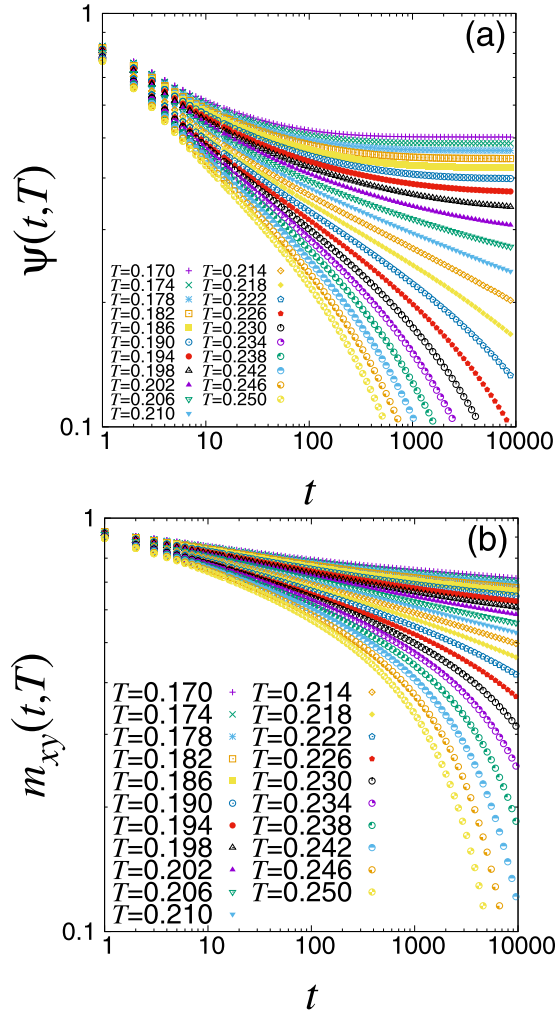

FIG. 10. Relaxation of the order parameters at $h = 5$ on the 2001×2000 triangular lattice plotted on a double-logarithmic scale. (a) The relaxation of ψ. (b) That of m_{xy}.

To evaluate error bars, the bootstrap method [27] is applied. Here we repeat the dynamical scaling analysis for 100 randomly chosen sets from relaxation data. We obtain 100 samples of transition temperature and dynamical exponent, T_c and λ_m, of ψ in the low-temperature range, those of ψ in the high-temperature range, and T_{KT} and λ_m of m_{xy} in the high-temperature range. The averaged T_c for the low and high temperature ranges are $T_c^L = 0.36642(2)$ and $T_c^H = 0.366414(9)$, respectively. Because these two temperatures are consistent with each other within the error bars, it is reasonable to conclude that $T_c = 0.36642(2)$. Similarly, T_{KT} averaged for the high-temperature range is given by $T_{KT} = 0.13638(7)$. These estimations are consistent with the previous results with $T_c = 0.364(1)$ for Z_3 and $T_{KT} = 0.138(3)$ for $O(2)$ [16]. Averaged λ_m of ψ in Eq. (3.4) and that of m_{xy} in Eq. (3.6) with error bar are also evaluated. The results are $\lambda_m = 0.0737(6)$ for ψ and $\lambda_m = 0.0692(3)$ for m_{xy}. Because these values characterize the dynamical behavior of an order parameter at T_c or T_{KT}, it cannot be compared with a previous study using EMCS. In the analysis of the phase transition at $h = 2$ (in the low field) using the series of the NER methods, we have confirmed

that the transition type and the transition temperature are consistent with previous studies [4,5,16]. This supports the present selection of the dynamical order parameters, Eqs. (2.9) and (2.10).

IV. HIGH-FIELD RANGE

A. Relaxation of order parameters

We apply the same analysis as in the previous section to the phase transition in the high-field range. ψ and m_{xy} are both used for that between the 2:1 canted phase and PM phase. We calculate the relaxation of them for several values of field; as an example, we show the results for $h = 5$ in detail. Figure 3(c) is selected as the initial state of relaxation. The conditions for the calculation are the same as those for the low field in Sec. III A. The relaxations for $h = 5$ are plotted in Fig. 10 with a double-logarithmic scale. We investigate a finite-size dependence of relaxation in this case. The relaxations of ψ and m_{xy} are calculated for several sizes at $(T, h) = (0.3, 3.5)$ to which the multicritical point is closely located [16], and a strong fluctuation is expected to appear. The results are plotted in Fig. 11. We confirm that the finite-size effect does not appear up to 10^4 MCSs on the 2001×2000 triangular lattice. Because we study the phase transitions for $h > 3.5$ away from this field, $h = 3.5$, the finite-size effect does not occur in our calculations, even in Fig. 10 for $h = 5$. Similarly to the low-field case, ψ in Fig. 10(a) shows a typical second-order transition like Eq. (3.1). As for m_{xy} in Fig. 10(b), it is not clear whether m_{xy} is relaxing toward a spontaneous order like Eq. (3.1) or with a power-law decaying like Eq. (3.2) in the low-temperature range.

B. Dynamical scaling analysis and discrimination of transition type

We examine the relaxation of m_{xy} in Fig. 10(b) by the use of the discrimination of the transition type introduced in Sec. III B. We select ten values of temperature in the high-temperature range of m_{xy} in Fig. 10(b), i.e., $T_1 = 0.214$, $T_2 = 0.218, \ldots, T_{10} = 0.250$. For each temperature, we choose several data points after 100 MCSs at regular intervals on $\ln(t)$. As in Sec. III B, three types of scalings are performed for chosen data points in order to discriminate the transition type. The result is shown in Fig. 12. It is expected that the values of τ_ℓ for T_ℓ $(\ell = 1, \ldots, 10)$ estimated without assuming an asymptotic form are the most reliable. As seen in Fig. 12, these values seem to be in good agreement with the curve obtained by using Eq. (3.5) for the second-order transition. Furthermore, the numerical difference between $\tau(T_\ell)$ with assuming functions and τ_ℓ without assuming a function are also evaluated. The residuals are calculated from Eq. (3.12) with $N_T = 10$ as $r_{2\mathrm{nd}} = 1.41 \times 10^{-3}$ for Eq. (3.5) and $r_{\mathrm{KT}} = 2.86 \times 10^{-1}$ for Eq. (3.7) indicating that the relaxation of m_{xy} in the high-temperature range shows a second-order transition. Therefore, that in the low-temperature range in Fig. 10(b) is also expected to exhibit a second-order transition instead of a KT transition. This means that the relaxation in the low-temperature range is not algebraic in our observation.

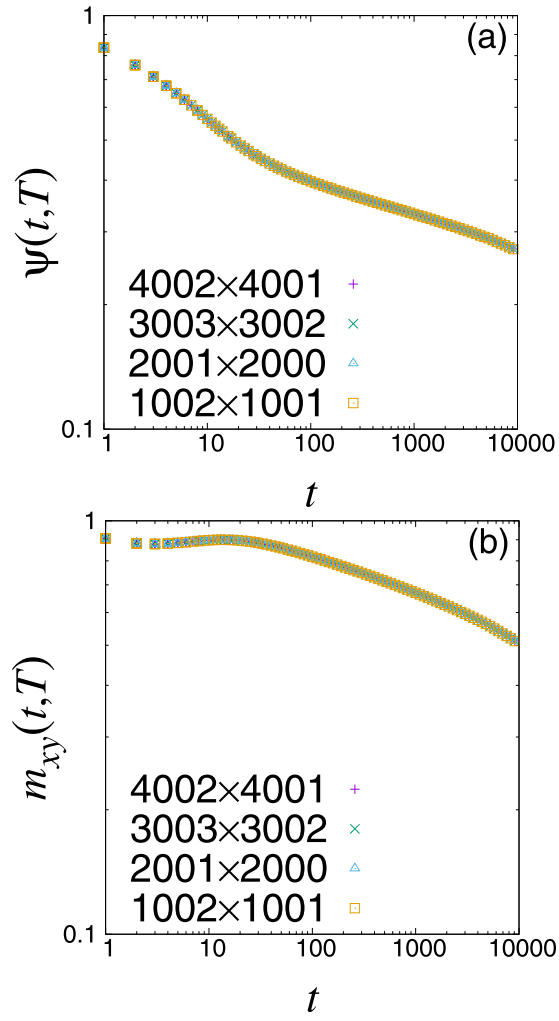

FIG. 11. The size dependence of relaxation at $(T, h) = (0.3, 3.5)$ close to the multicritical point. (a) The relaxation of ψ. (b) That of m_{xy}. For the case $L = 1001$, the relaxation coincides with those for larger sizes, 2000, 3002, 4001, up to 10^4 MCSs.

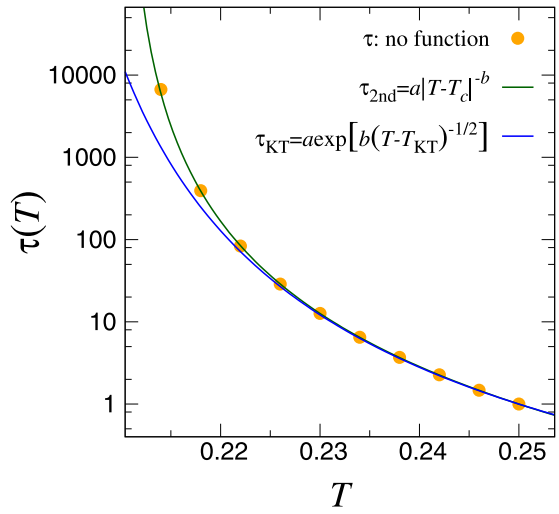

FIG. 12. Comparison of relaxation times estimated by three types of dynamical scaling for m_{xy} in Fig. 10(b) at $h = 5$. They are plotted versus T.

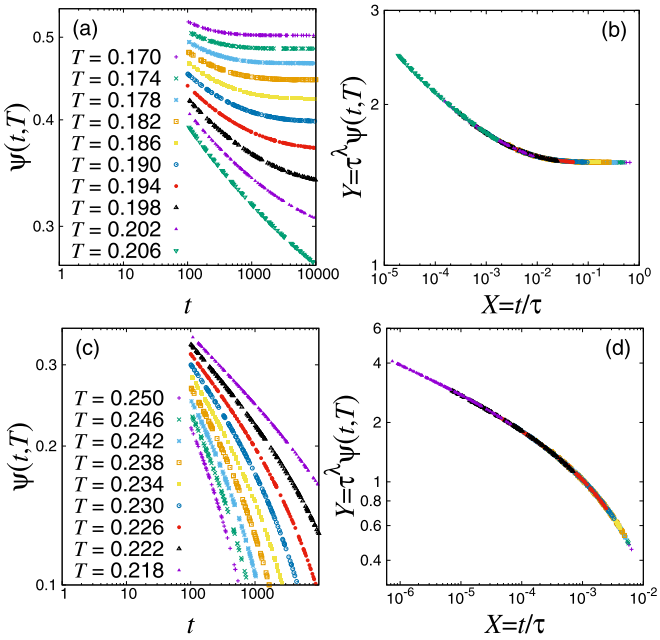

FIG. 13. (a) An example of randomly chosen relaxation data of ψ in the low-temperature range in Fig. 10(a), and (b) corresponding scaling plot. (c), (d) Those in the high-temperature range.

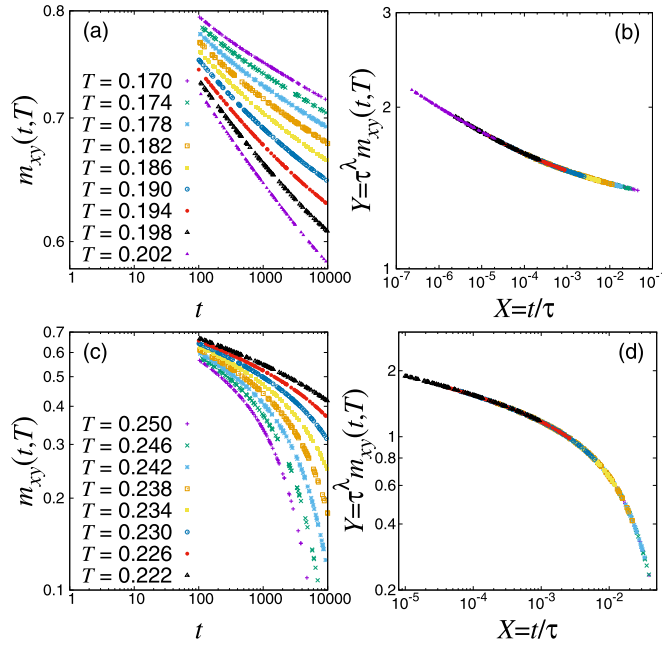

FIG. 14. (a) An example of randomly chosen relaxation data of m_{xy} in the low-temperature range in Fig. 10(b), and (b) corresponding scaling plot. (c), (d) Those in the high-temperature range.

C. Estimation of transition temperature and dynamical exponent

In this subsection, the transition temperature and dynamical exponent are estimated using the dynamical scaling analysis introduced in Sec. III B and performed in Sec. III C. Similarly to the low-field case, several temperatures are selected for the low and the high temperature ranges, respectively. For each selected temperature, several data points of ψ and m_{xy} are randomly chosen after 100 MCSs. Assuming an asymptotic form of relaxation time as the second-order transition type, Eq. (3.5), the dynamical scaling analysis is performed for ψ and m_{xy} to estimate T_c and λ_m. We note that in Sec. IV B, we have confirmed that the relaxation time of m_{xy} diverges with an asymptotic form closer to Eq. (3.5) than Eq. (3.7). Thus, Eq. (3.5) is applied not only to ψ but also to m_{xy}. The results are shown in Fig. 13 for ψ and in Fig. 14 for m_{xy}. There is no contradiction in using Eq. (3.5) for dynamical scaling of m_{xy} because the scaling plot for m_{xy} was achieved successfully in Fig. 14(b) even in the low-temperature range.

To estimate T_c precisely with error bars, the bootstrap method [27] is applied. The process is the same as in Sec. III C. The transition temperature of ψ is estimated as $T_c^L = 0.21169(4)$ from 100 randomly chosen samples in the low-temperature range and $T_c^H = 0.21391(8)$ from those in the high-temperature range; then we conclude $T_c = 0.213(1)$. Similarly, it is estimated for m_{xy} as $T_c^L = 0.20649(9)$ from 100 randomly chosen samples in the low-temperature range and $T_c^H = 0.21027(3)$ from those in the high-temperature range; then we conclude $T_c = 0.208(2)$. These are summarized in Table I together with the critical exponents estimated later. In a previous study [16], $T_c = 0.212(1)$ was concluded both for the Z_3 and the $O(2)$ symmetries. The present result for ψ is consistent with it, while that for m_{xy} is indicated slightly lower. We do not emphasize this difference based on our present results, because both values are close to each other and it is reasonable to consider them to be consistent with previous result. The transition temperatures are estimated in several fields other than $h = 5$. The result is shown in Fig. 15. In the above bootstrap analysis, the dynamical exponents for $h = 5$ are also estimated as $\lambda_m = 0.125(7)$ for ψ and $\lambda_m = 0.060(5)$ for m_{xy}. We note that λ_m defined in Eq. (3.4) is associated with the order parameter, and the above two values should be distinct from each other. They are also estimated in other fields. The result is presented in Fig. 16. As seen in Fig. 16, λ_m of ψ increases as a function of h. Conversely, that of

TABLE I. Estimated transition temperatures and critical exponents at $h = 5$ are summarized together with those obtained in a previous study [16].

	T_c	λ_m	z	ν	β	η
ψ	0.213(1)	0.125(7)	1.96(2)	1.76(4)	0.40(2)	0.47(2)
m_{xy}	0.208(2)	0.060(5)	1.97(2)	1.95(3)	0.22(2)	0.23(2)
Ref. [16] for Z_3	0.212(1)	n/a	n/a	2.0(2)	0.50(5)	0.50(5)
Ref. [16] for $O(2)$	0.212(1)	n/a	n/a	n/a	n/a	0.27(2)

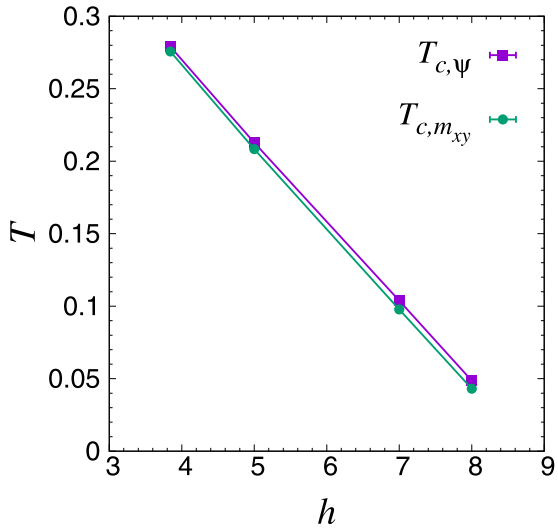

FIG. 15. Transition temperatures of ψ and m_{xy} are plotted versus h.

m_{xy} seems almost constant within the error bars. The critical property of m_{xy} appears to be distinct from that of ψ.

D. Relaxation of fluctuations for critical exponents

To investigate the universality class, we estimate critical exponents for ψ and m_{xy}. In the NER analysis, the critical exponents are estimated by the use of the relaxation of NER functions which express fluctuations [19]. We consider the following two types of NER functions:

$$f_{mm}(t,T) = N\left\{\frac{\langle m(t,T)^2\rangle}{\langle m(t,T)\rangle^2} - 1\right\}, \tag{4.1}$$

$$f_{me}(t,T) = N\left\{\frac{\langle m(t,T)e(t,T)\rangle}{\langle m(t,T)\rangle\langle e(t,T)\rangle} - 1\right\}, \tag{4.2}$$

where $e(t,T)$ is the energy per site and m is one of the order parameters, i.e., ψ or m_{xy}. These functions are expected to

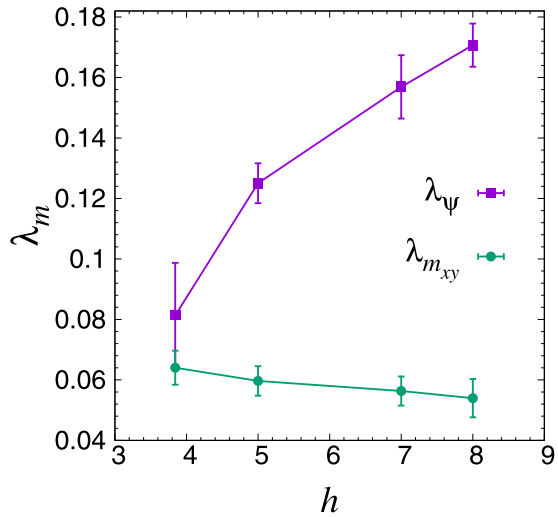

FIG. 16. Dynamical exponents of ψ and m_{xy} are plotted versus h.

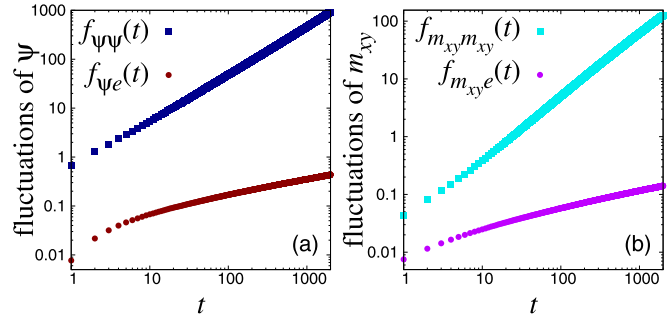

FIG. 17. Relaxation of the NER functions at $h = 5$: (a) in terms of ψ and (b) in terms of m_{xy}.

exhibit power-law divergences at the transition temperature [19] as follows:

$$f_{mm}(t,T_c) \sim t^{\lambda_{mm}}, \tag{4.3}$$

$$f_{me}(t,T_c) \sim t^{\lambda_{me}}, \tag{4.4}$$

where λ_{mm} and λ_{me} are dynamical exponents for these functions, which are related to the conventional critical exponents as

$$\lambda_{mm} = d/z, \tag{4.5}$$

$$\lambda_{me} = 1/z\nu. \tag{4.6}$$

Here we define the local exponents of Eqs. (3.1), (4.3), and (4.4) at T_c as follows:

$$\lambda_m(t) = -\frac{d\ln m(t,T_c)}{d\ln t}, \tag{4.7}$$

$$\lambda_{mm}(t) = \frac{d\ln f_{mm}(t,T_c)}{d\ln t}, \tag{4.8}$$

$$\lambda_{me}(t) = \frac{d\ln f_{me}(t,T_c)}{d\ln t}, \tag{4.9}$$

and then the local critical exponents are defined by

$$z(t) = \frac{d}{\lambda_{mm}(t)}, \tag{4.10}$$

$$\nu(t) = \frac{\lambda_{mm}(t)}{d\lambda_{me}(t)}, \tag{4.11}$$

$$\beta(t) = \frac{\lambda_m(t)}{\lambda_{me}(t)}, \tag{4.12}$$

$$\eta(t) = \frac{2d\lambda_m(t)}{\lambda_{mm}(t)}, \tag{4.13}$$

where the corresponding critical exponents are evaluated as $t \to \infty$. We apply the heat bath algorithm [25] to this system and calculate Eqs. (4.1), (4.2), and (3.1) at T_c estimated above up to 2000 MCSs. The system size is 1002×1001 and the skew boundary condition is used. We simulate about 1.25×10^6 samples for averaging. As seen in Fig. 11, the finite-size effect was not observed in the 1002×1001 lattice up to 2000 MCSs. As an example, the obtained relaxation of NER functions for ψ and m_{xy} at $h = 5$ are plotted in Fig. 17. To obtain critical exponents at $t \to \infty$, we evaluate logarithmic derivatives for f_{mm} and f_{me} and calculate local exponents defined by Eqs. (4.10), (4.11), (4.12), and (4.13)

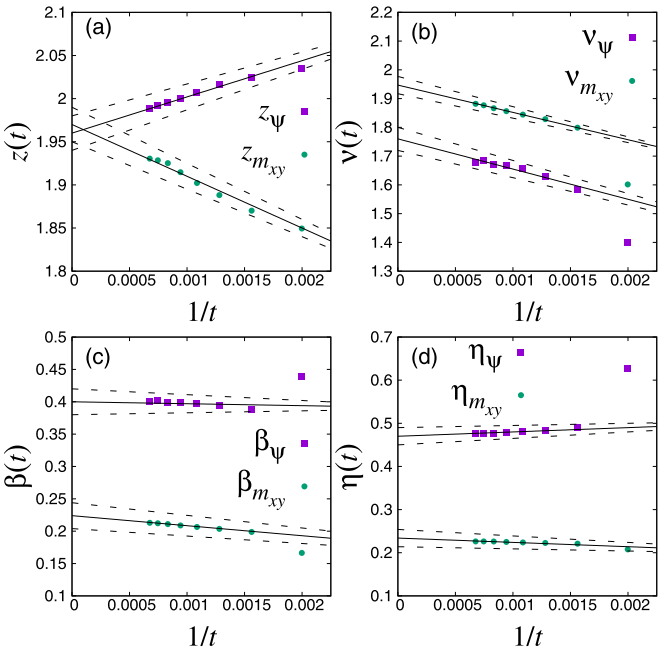

FIG. 18. Local critical exponents at $h = 5$: (a) $z(t)$, (b) $\nu(t)$, (c) $\beta(t)$, and (d) $\eta(t)$ in terms of ψ and m_{xy}. The best fittings are indicated by solid lines, and broken lines are guides to the eye for errors to see the asymptotic behaviors.

for several values of t, which are plotted as a function of $1/t$ in Fig. 18. The estimated exponents for $h = 5$ are summarized in Table I. Critical exponents for other fields are also estimated and presented in Fig. 19 together with those from a previous study [16].

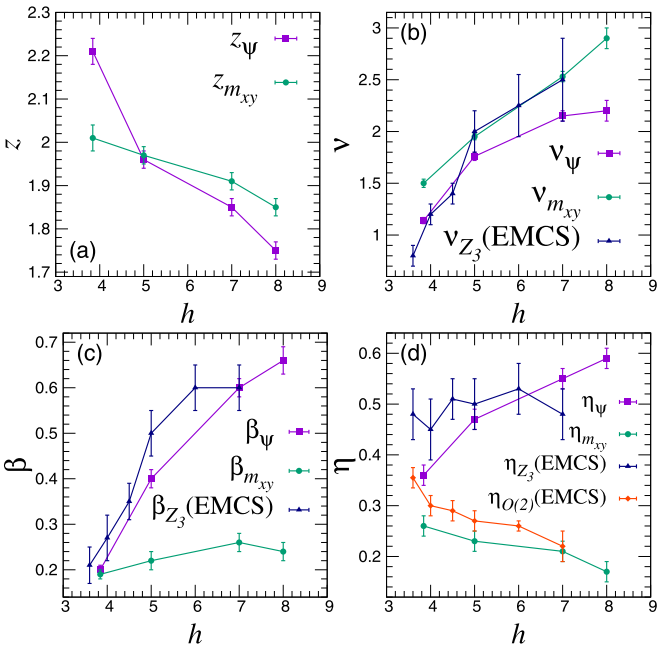

FIG. 19. Critical exponents plotted versus h: (a) z, (b) ν, (c) β, and (d) η. Exponents with the subscripts Z_3, $O(2)$, and (EMCS) were estimated in a previous study [16].

Next, we discuss a comparison between these studies. Note that the dynamics and the transition in terms of m_{xy} are not compared with previous research [16] where it has not been studied. It has been pointed out that exponents ν, β, and η of Z_3 which were estimated in a previous study change depending on h [see Figs. 19(b)–19(d)], which reveals that the transition in terms of the Z_3 symmetry does not belong to any universality class [16]. This property is confirmed by the present results. β and η of ψ are almost consistent with those of a previous study, while ν of ψ are deviated in a higher field range. The reason that ν of m_{xy} are rather close to that of Z_3 estimated in a previous study in a higher field range is not clear. It is deduced that the transition in terms of m_{xy} for S^x-S^y components does not belong to any universality class because the critical exponents of m_{xy} also change continuously. While exponents of ψ and m_{xy} change continuously, their values are clearly different, especially in β and η. Their difference does not seem to be due to composite operators because we could not find a simple ratio between these exponents. Thus, the transition in terms of m_{xy} is distinct from that of ψ. Because m_{xy} has not been investigated in previous studies, attention should be paid to the interpretation of these behaviors.

V. DISCUSSION AND CONCLUSION

In this study, we applied the nonequilibrium relaxation method (NER) to the antiferromagnetic triangular Heisenberg system in a uniform field. The relaxation of the order parameters was calculated using a heat bath algorithm from the appropriate ordered spin state, and dynamical scaling analysis was applied. We estimated transition temperatures and determined the transition types. The critical exponents in the transition between the 2:1 canted phase and PM phase were estimated by calculating the relaxation of the NER functions. In the low field, at $h = 2$, it was confirmed that the relaxation of the order parameters ψ and m_{xy} indicates a typical second-order transition and a KT transition, respectively. The transition temperatures are distinct, which is consistent with the results of previous studies [4,5,16]. In the high-field range ($3 \lesssim h \lesssim 9$), the relaxation of ψ indicates a second-order transition, and the critical exponents change continuously as a function of field and do not belong to any universality class. These results are consistent with a previous study [16]. In contrast to ψ, we obtain the further picture in terms of m_{xy} for the S^x-S^y components around the field axis in the transition between the 2:1 canted phase and PM phase. A previous study [16] argued that the ordering of the S^x-S^y components about rotational symmetry is algebraic in the low-temperature ordered phase and that this transition is not a KT transition. We confirm that it is not a KT transition as proven by the relaxation time diverging with an asymptotic form for a second-order transition rather than a KT transition (see Fig. 12). Furthermore, it was shown that in the low-temperature phase, the S^x-S^y components do not have an algebraic order provided by dynamical scaling in the low-temperature range using Eq. (3.5), as shown in Fig. 14(b). The critical exponents in terms of m_{xy} for the S^x-S^y components change continuously as a function of the field (see Fig. 19).

We discuss the unexpected behavior that the relaxation time of m_{xy} shows a divergence as a second-order transition

Eq. (3.5) in the high-field range. This result appears to contradict the Mermin-Wagner theorem [29,30], which defies the ordering in continuous spin systems with a continuous symmetry in two dimensions. We utilized this order parameter for the following four reasons: First, we used this order parameter in accordance with the results in the low-field range, in which the transition temperature and transition type obtained using m_{xy} are consistent with those of previous studies [4,5,16]. Second, the order parameter m_{xy} is composed of the S^x-S^y components and so is the spin stiffness used in Ref. [16], which was used to detect the transition, while the forms of these components are a little different. Third, dynamical scaling analysis is consistently performed in keeping with the dynamical scaling law, Eq. (3.3), as shown in Figs. 14(b) and 14(d). The fourth reason, as seen in Fig. 19(d), is that η of m_{xy} for the S^x-S^y components is similar to that of a previous study. With all these reasons, m_{xy}, the projection to the spin structure in the zero-temperature limit, would be inappropriate as an order parameter for the S^x-S^y components with rotational symmetry. There is another possibility that the breaking of the Z_3 symmetry for the S^z components affects critical properties of the S^x-S^y components. This has been highlighted in a previous study [16], which concluded that the phase transition between the 2:1 canted phase and PM phase is a single transition in which the S^z components and S^x-S^y components become critical at the same temperature. In such a case, the fluctuation generated around the transition for the Z_3 and $O(2)$ symmetry are coupled long-range interactions. If this is the case, the standard Mermin-Wagner theory cannot be applied. Because the two transition temperatures are clearly separated, the ordering behaviors for pure short-range interactions appear for the low field, i.e., the second-order transition for Z_3 symmetry and the KT transition for $O(2)$ symmetry. Conversely, for the high field, because the S^z components affect the S^x-S^y components, it is deduced that the relaxation time of m_{xy} diverges with an asymptotic form of the second-order transition Eq. (3.5) instead of the KT transition Eq. (3.7). Further research is required to resolve this issue.

We hope that our results enrich the discussion on symmetry breaking in condensed matter physics and statistical physics.

ACKNOWLEDGMENTS

This research was supported by JSPS KAKENHI Grants No. 15K05205 and No. 19K03666. The authors are grateful to Ryogo Tobise, Tsutomu Momoi, and Yuka Nakamura for valuable discussions, support, and comments. The authors are also grateful to the Supercomputer Center at the Institute for Solid State Physics, University of Tokyo, for the use of its facilities.

[1] H. Diep *et al.*, *Frustrated Spin Systems* (World Scientific, 2013).
[2] O. A. Starykh, Rep. Prog. Phys. **78**, 052502 (2015).
[3] H. Kawamura and S. Miyashita, J. Phys. Soc. Jpn. **53**, 4138 (1984).
[4] H. Kawamura and S. Miyashita, J. Phys. Soc. Jpn. **54**, 4530 (1985).
[5] M. Gvozdikova, P. Melchy, and M. Zhitomirsky, J. Phys.: Condens. Matter **23**, 164209 (2011).
[6] P. W. Anderson, Mater. Res. Bull. **8**, 153 (1973).
[7] B. Bernu, C. Lhuillier, and L. Pierre, Phys. Rev. Lett. **69**, 2590 (1992).
[8] L. Capriotti, A. E. Trumper, and S. Sorella, Phys. Rev. Lett. **82**, 3899 (1999).
[9] S. Sachdev, Phys. Rev. B **45**, 12377 (1992).
[10] H. Kawamura and M. Kikuchi, Phys. Rev. B **47**, 1134 (1993).
[11] A. Chubokov and D. Golosov, J. Phys.: Condens. Matter **3**, 69 (1991).
[12] L. E. Svistov, A. I. Smirnov, L. A. Prozorova, O. A. Petrenko, A. Micheler, N. Büttgen, A. Y. Shapiro, and L. N. Demianets, Phys. Rev. B **74**, 024412 (2006).
[13] R. Ishii, S. Tanaka, K. Onuma, Y. Nambu, M. Tokunaga, T. Sakakibara, N. Kawashima, Y. Maeno, C. Broholm, D. Gautreaux *et al.*, Europhys. Lett. **94**, 17001 (2011).
[14] H. Kawamura, A. Yamamoto, and T. Okubo, J. Phys. Soc. Jpn. **79**, 023701 (2010).
[15] T. Okubo and H. Kawamura, J. Phys. Soc. Jpn. **79**, 084706 (2010).
[16] L. Seabra, T. Momoi, P. Sindzingre, and N. Shannon, Phys. Rev. B **84**, 214418 (2011).
[17] V. Berezinsky, Zh. Eksp. Teor. Fiz. **61**, 610 (1972).
[18] J. M. Kosterlitz and D. J. Thouless, J. Phys. C: Solid State Phys. **6**, 1181 (1973).
[19] Y. Ozeki and N. Ito, J. Phys. A: Math. Theor. **40**, R149 (2007).
[20] Y. Ozeki and N. Ito, Phys. Rev. B **68**, 054414 (2003).
[21] Y. Ozeki, S. Yotsuyanagi, T. Sakai, and Y. Echinaka, Phys. Rev. E **89**, 022122 (2014).
[22] Y. Ozeki and N. Ito, Phys. Rev. B **64**, 024416 (2001).
[23] H. Kawamura, J. Phys. Soc. Jpn. **53**, 2452 (1984).
[24] E. Rastelli, A. Tassi, A. Pimpinelli, and S. Sedazzari, Phys. Rev. B **45**, 7936 (1992).
[25] J. A. Olive, A. P. Young, and D. Sherrington, Phys. Rev. B **34**, 6341 (1986).
[26] The skew boundary condition is a practical choice to facilitate program implementation, and its effect is expected to disappear in the thermodynamic limit.
[27] Y. Echinaka and Y. Ozeki, Phys. Rev. E **94**, 043312 (2016).
[28] Y. Ozeki, A. Matsuda, and Y. Echinaka, Phys. Rev. E **99**, 012116 (2019).
[29] N. D. Mermin and H. Wagner, Phys. Rev. Lett. **17**, 1133 (1966).
[30] N. D. Mermin, J. Math. Phys. **8**, 1061 (1967).